Effects of melatonin on dopaminergic neuron development via IP3-mediated mitochondrial Ca2+ regulation in autism spectrum disorder

董, 双山

Biochemical and Biophysical Research Communications 681 (2023) 7–12

Contents lists available at ScienceDirect

Biochemical and Biophysical Research Communications

journal homepage: www.elsevier.com/locate/ybbrc

Effects of melatonin on dopaminergic neuron development via IP3-mediated mitochondrial Ca^{2+} regulation in autism spectrum disorder

Shuangshan Dong [a], Takashi Kifune [a], Hiroki Kato [b], Lu Wang [a], Jun Kong [a], Yuta Hirofuji [a], Xiao Sun [a,1], Hiroshi Sato [a], Yosuke Ito [a], Takahiro A. Kato [c], Yasunari Sakai [d], Shouichi Ohga [d], Satoshi Fukumoto [a,**], Keiji Masuda [a,*]

[a] Section of Oral Medicine for Children, Division of Oral Health, Growth and Development, Faculty of Dental Science, Kyushu University, Maidashi 3-1-1, Higashi-Ku, Fukuoka, 812-8582, Japan
[b] Department of Molecular Cell Biology and Oral Anatomy, Kyushu University Graduate School of Dental Science, Maidashi 3-1-1, Higashi-Ku, Fukuoka, 812-8582, Japan
[c] Department of Neuropsychiatry, Graduate School of Medical Sciences, Kyushu University, Maidashi 3-1-1, Higashi-Ku, Fukuoka, 812-8582, Japan
[d] Department of Pediatrics, Graduate School of Medical Sciences, Kyushu University, Maidashi 3-1-1, Higashi-Ku, Fukuoka, 812-8582, Japan

ARTICLE INFO

Keywords:
Melatonin
Autism spectrum disorder
Mitochondria
Calcium
Neurodevelopment

ABSTRACT

Melatonin entrainment of suprachiasmatic nucleus-regulating circadian rhythms is mediated by MT1 and MT2 receptors. Melatonin also has neuroprotective and mitochondrial activating effects, suggesting it may affect neurodevelopment. We studied melatonin's pharmacological effects on autism spectrum disorder (ASD) neuropathology. Deciduous tooth-derived stem cells from children with ASD were used to model neurodevelopmental defects and differentiated into dopaminergic neurons (ASD-DNs) with or without melatonin. Without melatonin, ASD-DNs had reduced neurite outgrowth, mitochondrial dysfunction, lower mitochondrial Ca^{2+} levels, and Ca^{2+} accumulation in the endoplasmic reticulum (ER) compared to control DNs from typically developing children-derived stem cells. Melatonin enhanced IP3-dependent Ca^{2+} release from ER to mitochondria, improving mitochondrial function and neurite outgrowth in ASD-DNs. Luzindole, an MT1/MT2 antagonist, blocked these effects. Thus, melatonin supplementation may improve dopaminergic system development in ASD by modulating mitochondrial Ca^{2+} homeostasis via MT1/MT2 receptors.

1. Introduction

Autism spectrum disorder (ASD) is a neurodevelopmental disorder with social and communication impairments and repetitive behaviors [1]. Various genetic and environmental risk factors for ASD have been identified [2,3]. ASD's neuropathology hypotheses include mitochondrial dysfunction [4], dopaminergic dysregulation [5,6], and intracellular Ca^{2+} dysregulation [7]. Mitochondrial dysfunction has been linked to impaired neurite development in dopaminergic neurons (DNs) using stem cells derived from children with ASD [8]. However, ASD neuropathology mechanisms and effective treatments remain unknown.

Melatonin (MLT)-related sleep and circadian rhythm disturbances contribute to ASD neuropathology [9,10]. The hypothalamic suprachiasmatic nucleus (SCN) controls melatonin release, inducing sleep [11,12]. MLT activates G protein-coupled receptors (GPCRs), MT1 and MT2, providing feedback to entrain circadian rhythms [13]. MLT-timed administration enhances sleep quality in patients with ASD [14]. MLT impacts pathological conditions through antioxidant, neuroprotective, and mitochondrial activation effects [15]. MT1 and MT2 are extensively present in the brain [16]. MLT may aid brain development and lessen ASD symptoms. Yet, the mechanisms and significance of MLT's impact on neurodevelopment are unclear.

Stem cells from human exfoliated deciduous teeth (SHEDs) can differentiate into dopaminergic neurons (DNs) due to their neural crest origin and neuroplasticity [17–20]. Since the midbrain dopaminergic system is involved in many brain functions [21], patient-derived SHEDs are a promising cellular model for studying dopamine-related

* Corresponding author.
** Corresponding author.
E-mail addresses: fukumoto@dent.kyushu-u.ac.jp (S. Fukumoto), kemasuda@dent.kyushu-u.ac.jp (K. Masuda).
[1] Present address: Key Laboratory of Shaanxi Province for Craniofacial Precision Medicine Research, and Department of Pediatric Dentistry, College of Stomatology, Xi'an Jiaotong University, No. 98, Xiwu Road, Xincheng District, Xi'an, 710004, China.

https://doi.org/10.1016/j.bbrc.2023.09.050
Received 25 August 2023; Received in revised form 15 September 2023; Accepted 19 September 2023
Available online 19 September 2023

Abbreviations

ASD	autism spectrum disorder
DNs	dopaminergic neurons
ER	endoplasmic reticulum
GPCR	G protein-coupled receptor
$G\alpha_i$	G protein α subunit i isoform
$G\alpha_{q/11}$	G protein α subunit q/11 isoform
Gβγ	G protein β and γ subunits
IP3	inositol 1,4,5-trisphosphate
IP3R	inositol 1,4,5-trisphosphate receptor
LZD	luzindole
MLT	melatonin
mtCU	mitochondrial calcium uniporter channel complex
PIP2	phosphatidylinositol 4,5-bisphosphate
PLCβ	phospholipase C β subfamily
RuR	ruthenium red
SHEDs	stem cells from human exfoliated deciduous teeth
XestC	xestospongin C

neuropathology [22]. Here, we used DNs differentiated from patient-derived SHEDs with or without MLT to assess MLT's effects on ASD neuropathology.

2. Materials and methods

2.1. SHED isolation, culture, and differentiation into dopaminergic neurons (DNs)

The Kyushu University Institutional Review Board for Human Genome/Gene Research (permission number: 678-03) approved human sample experiments following the Declaration of Helsinki. Written informed consent was obtained from parents. Deciduous teeth were collected from three typically developing children and three with ASD, aged 4–7 years.

SHEDs were isolated and cultured in alpha-modified Eagle's Medium (Nacalai Tesque, Kyoto, Japan) with 15% fetal bovine serum (Sigma-Aldrich, St. Louis, MO, USA), 100 μM L-ascorbic acid 2-phosphate (Wako Pure Chemical Industries, Osaka, Japan), 250 μg/mL fungizone (Thermo Fisher Scientific, Waltham, MA, USA), 100 U/mL penicillin, and 100 μg/mL streptomycin (Nacalai Tesque) at 37 °C in a 5% CO_2 atmosphere [8,23].

SHED differentiation to DNs was performed using a two-step procedure [8,23]. In the first step, 1.5×10^5 SHEDs were seeded in a six-well culture plate (Corning, Corning, NY, USA) and cultured. After 24 h, cells were cultured in Dulbecco's Modified Eagle's Medium (first-step; #08456-65; DMEM, Nacalai Tesque), supplemented with 20 ng/mL epidermal growth factor (PeproTech, East Windsor, NJ, USA), 20 ng/mL basic fibroblast growth factor (Peprotech), and 1% N-2 supplement (Thermo Fisher Scientific, Waltham, MA, USA) for 2 d at 37 °C under 5% CO_2. In the second step, the medium was replaced with a neurobasal medium (Thermo Fisher Scientific) supplemented with 2% B27 supplement (Thermo Fisher Scientific), 1 mM dibutyryladenosine 3, 5-cyclic monophosphate (Nacalai Tesque), 0.5 mM 3-isobutyl-1-methyl-xanthine (Wako Pure Chemical Industries), and 200 μM ascorbic acid (Nacalai Tesque). Cells were incubated for 5 d at 37 °C under 5% CO_2.

2.2. Melatonin (MLT), luzindole (LZD), and xestospongin C (XestC) treatment

MLT (1 μM; Sigma-Aldrich) and LZD (10 μM; Wako Pure Chemical Industries), were added to the second-step medium used for DN differentiation. XestC (5 μM; Cayman Chemical Company, Ann Arbor, MI, USA) was added on the last day of DN differentiation, and cells were incubated for 4 h at 37 °C under 5% CO_2 before analysis.

2.3. Analyses of neuronal morphology by immunocytochemistry

DNs were cultured on cover glass and fixed with 4% paraformaldehyde in 0.1 M sodium phosphate buffer (pH 7.4) for 10 min at 25 °C and subsequently permeabilized with 0.1% Triton X-100 in phosphate-buffered saline (PBS) for 5 min at 25 °C. Cells were blocked with 2% BSA in PBS for 20 min at 25 °C and subsequently incubated with the following primary antibodies for 90 min at 25 °C: mouse monoclonal anti-tyrosine hydroxylase (TH; #66334-1-Ig; Proteintech, Rosemont, IL, USA), and mouse monoclonal anti-β-tubulin III (#T8578; Sigma-Aldrich). Cells were subsequently incubated with Alexa Fluor-conjugated secondary antibodies (Thermo Fisher Scientific) for 1 h at 25 °C in the dark. Nuclei were counterstained with 1 μg/mL 4′,6-diamidino-2-phenylindole dihydrochloride (DAPI; Dojindo, Kumamoto, Japan) in PBS for 5 min at 25 °C. The cover glass was then mounted on slides using ProLong Diamond mounting medium (Thermo Fisher Scientific). Fluorescence images were acquired using CFI Plan Apochromat Lambda 20 ×, 60 ×, and 100 × objective lenses on a Nikon C2 confocal microscope (Nikon, Tokyo, Japan).

To measure the maximum neurite length and total number of neurite branches, TH- and DAPI-stained pictures were acquired, and 30 cells were analyzed using the Neurite Outgrowth module in MetaMorph software version 7.8 (Molecular Devices, San Jose, CA, USA).

2.4. Quantitative and semi-quantitative reverse transcription polymerase chain reaction (RT-PCR)

Total RNA was extracted from cells using RNeasy Mini Kit (Qiagen, Hilden, Germany). First-strand cDNA was synthesized using RevaTra Ace qPCR RT Master Mix (Toyobo, Osaka, Japan). *MT2* expression was analyzed using GoTaq qPCR Master Mix (Promega, Madison, WI, USA), and QuantStudio 3 Real-Time PCR System (Thermo Fisher Scientific) was used for quantitative real-time PCR. Relative expression of target genes was analyzed using the comparative threshold cycle method via normalization to 18S rRNA levels. The primer set sequences were: MT2, 5′-TGC TCA GGA ACC GCA AGC TC-3′ (forward) and 5′-GTA GGG GTA GAA GGC CAC CA-3′ (reverse); 18S rRNA, 5′-CGG CTA CCA CAT CCA AGG AA-3′ (forward) and 5′-GCT GGA ATT ACC GCG GCT-3′ (reverse).

To analyze *MT1* expression, semi-quantitative PCR was performed using GoTaq (Promega). Amplified target gene fragments were electrophoresed using agarose gel electrophoresis and detected using Gel Green (Biotium, Fremont, CA, USA). Fluorescence images were acquired using SK-470 fluorescence microscope (BIO CRAFT, Tokyo, Japan). Fluorescence intensity of each target gene was measured using ImageJ software. Relative expression of target genes was normalized to that of 18S rRNA. The primer set sequences were: MT1, 5′-GCG TCC TCA TCT TCA CCA TC-3′ (forward) and 5′-ACG GAT AAA TGG CCA CCA CC-3′ (reverse); 18S rRNA, 5′-CGG CTA CCA CAT CCA AGG AA-3′ (forward) and 5′-GCT GGA ATT ACC GCG GCT-3′ (reverse).

2.5. Measurement of mitochondrial membrane potential (MMP)

MMP was measured using MMP indicator JC-1 (Wako Pure Chemical Industries) after differentiation into DNs. DNs were incubated with 1 μM JC-1 for 10 min. TrypLE Express (Thermo Fisher Scientific) detached cells from the culture plates, and a FACSCalibur (BD Biosciences, Franklin Lakes, NJ, USA) measured JC-1 red and green signals. The geometric means of red and green fluorescence were measured using Cell Quest 3.3 (BD Biosciences), and the ratio of red/green fluorescence was calculated.

2.6. Analysis of intracellular adenosine triphosphate (ATP) levels

The CellTiter-Glo Luminescent Cell Viability Assay (Promega) measured intracellular ATP levels after cells were harvested in ice-cold PBS. The luminescence signal was measured using SpectraMax iD3 Microplate Reader (Molecular Devices).

2.7. Analyses of mitochondrial and endoplasmic reticulum (ER) Ca^{2+} levels

To measure Ca^{2+} level per mitochondrion, cells were cultured in μ-dishes (ibidi, Munich, Germany), followed by incubation with 10 μM Rhod-2 AM (Dojindo) and 20 nM MitoTracker Green (Thermo Fisher Scientific) for 45 min. Fluorescent images were acquired using a Nikon C2 confocal microscope, and the Rhod-2 AM fluorescence intensity was divided by MitoTracker Green intensity.

To measure ER Ca^{2+} levels, cells were incubated with 1 μM Mag-Fluo-4 AM (AAT Bioquest, Sunnyvale, CA, USA) for 45 min. Fluorescence images were acquired using a Nikon C2 confocal microscope (Nikon). NIS-Elements software (Nikon) was used to measure the fluorescent intensity of five images per case.

2.8. Measurement of inositol 1,4,5-trisphosphate (IP3)

IP3 was measured using IP3 ELISA kit (Elabscience, Houston, TX, USA), following the manufacturer's instructions. Cells (2×10^6) were dissolved in 200 μL PBS and sonicated 20 times with Bioruptor UCD-3000 (CosmoBio, Tokyo, Japan) at 4 °C for 20 s. Subsequently, the cells were centrifuged at 17,500×*g* for 10 min at 4 °C, and the supernatants were collected. The IP3 ELISA kit used 50 μL supernatant; absorbance was measured at 450 nm using ARVO X3 (PerkinElmer, Waltham, MA, USA).

2.9. Statistical analyses

Statistical analyses were performed using Student's *t*-tests or one-way ANOVA with Prism9 (GraphPad, San Diego, CA, USA). Values are presented as the mean ± standard error of the mean (SEM). Statistical significance was set at $p < 0.05$.

3. Results

3.1. Melatonin was effective in ASD-DN development

Control-SHEDs and patient-derived SHEDs were differentiated to DNs (Ctrl-DNs and ASD-DNs, respectively). Western blot analysis showed similar protein expression of DN markers in both groups without MLT (Fig. S1). In this condition, ASD-DNs had lower neurite length and branch number than Ctrl-DNs (Fig. 1A, Fig. S2). MLT stimulated neurite outgrowth in ASD-DNs (Fig. 1A, Fig. S2). To investigate MT1 and MT2 receptor involvement, luzindole (LZD) [24], a non-selective MT1/MT2 antagonist was used (Fig. 1A, Fig. S2). LZD blocked MLT's effect on neurite outgrowth (Fig. 1A, Fig. S2). RT-PCR analysis showed similar MT1 and MT2 signals in Ctrl- and ASD-DNs (Fig. 1B, Fig. S3). Thus, MLT activated MT1 and MT2, aiding ASD-DN neurite growth.

3.2. Melatonin was effective in Ca^{2+}-mediated mitochondrial activation in ASD-DNs

To assess MLT's effect on mitochondrial function, MMP and ATP levels were measured. Without MLT, both were lower in ASD-DNs than Ctrl-DNs (Fig. 2A, Fig. S4). MLT increased MMP and ATP levels in ASD-DNs, which LZD blocked (Fig. 2A, Fig. S4). Mitochondrial Ca^{2+} levels associated with oxidative phosphorylation were then measured. Without MLT, ASD-DNs had lower mitochondrial Ca^{2+} levels than Ctrl-DNs (Fig. 2B, Fig. S5). MLT restored mitochondrial Ca^{2+} levels in ASD-DNs, but LZD blocked this effect (Fig. 2B, Fig. S5). These data suggested the important role of MLT in Ca^{2+}-mediated mitochondrial activation in

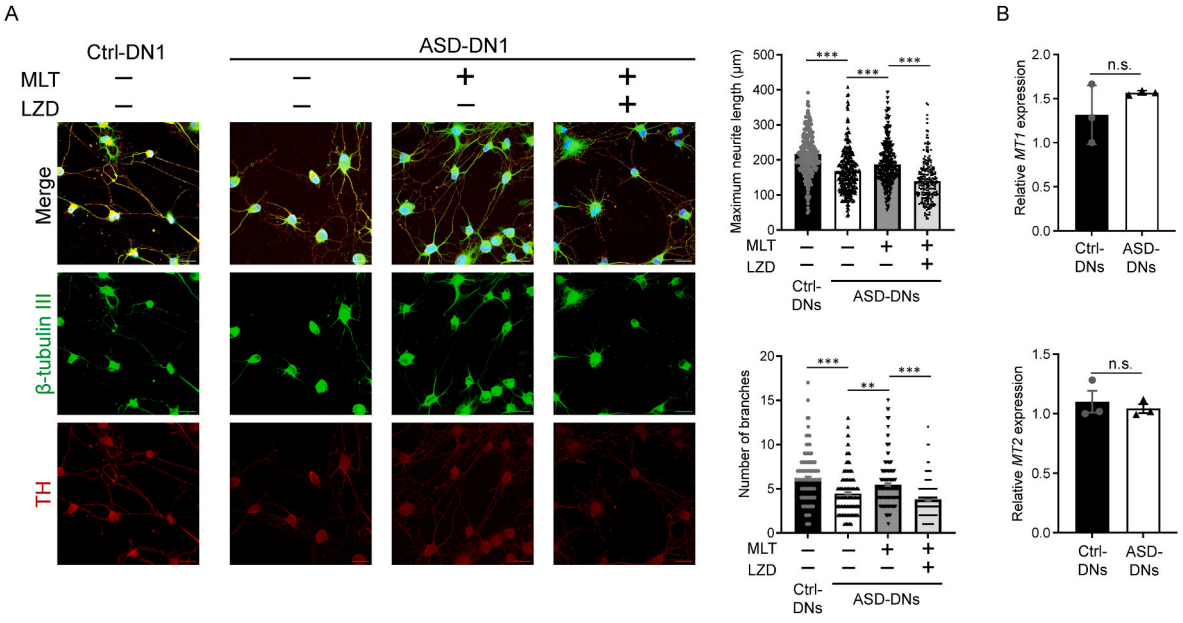

Fig. 1. Effect of melatonin (MLT) on neurite outgrowth in patient-derived dopaminergic neurons (DNs). Stem cells from human exfoliated deciduous teeth (SHEDs) were differentiated into DNs in the absence or presence of MLT and luzindole (LZD). (A) DNs were visualized via immunofluorescence microscopy using anti-β-tubulin III and anti-TH antibodies. Nuclei were counter-stained with 4′,6-diamidino-2-phenylindole dihydrochloride (DAPI). Control (Ctrl)-DN1 and autism spectrum disorder (ASD)-DN1 are shown as representative examples. Scale bars = 25 μm. Maximum neurite length and the total number of branches per DN were measured. The mean ± standard error of the mean (SEM) was calculated after analyzing 30 cells from three independent experiments. (B) mRNA expression levels of MT1 and MT2 were measured using semi-quantitative and quantitative polymerase chain reaction, respectively. The mean ± SEM was calculated after analyzing three Ctrl- and ASD-DNs. n.s., not significant; $^{**}p < 0.01$, $^{***}p < 0.001$.

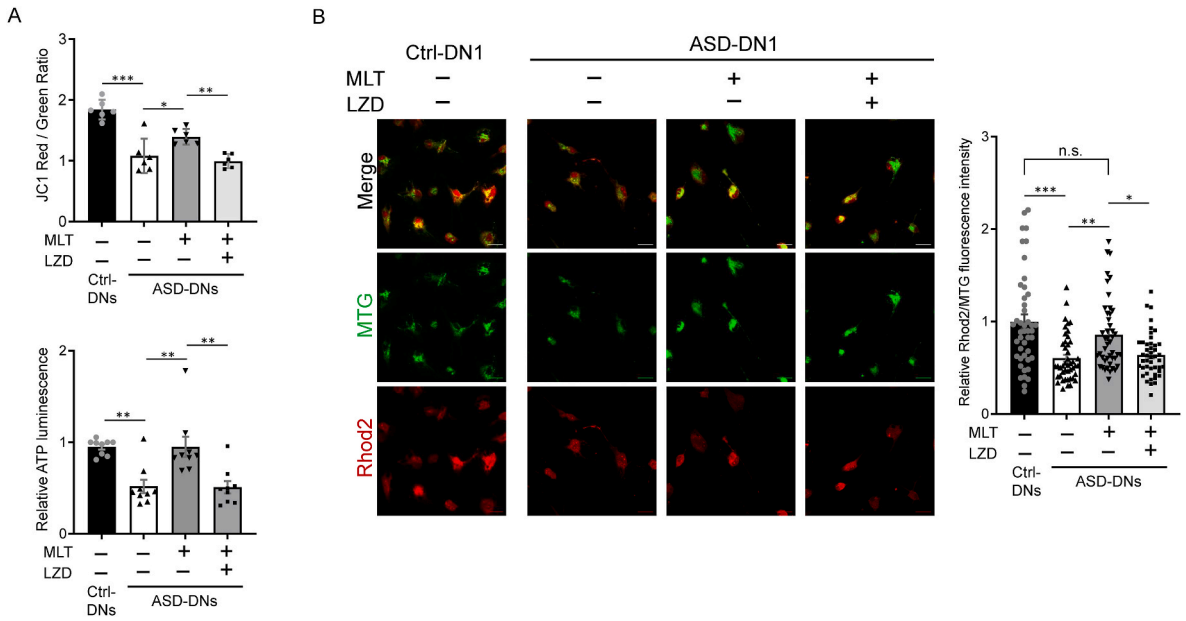

Fig. 2. Effect of MLT on mitochondrial activity and mitochondrial Ca^{2+} levels in patient-derived dopaminergic neurons (DNs). SHEDs were differentiated into DNs in the absence or presence of MLT and LZD. (A) Mitochondrial membrane potential (MMP) and adenosine triphosphate (ATP) levels in DNs were measured. The mean ± SEM was obtained from two (MMP) and three (ATP levels) independent experiments. (B) DNs stained with MitoTracker Green (MTG) and Rhod2 were observed using confocal microscopy. Scale bars = 25 μm. Fluorescence intensity of Rhod2 was divided by that of MTG to measure the Ca^{2+} level per mitochondrion. The mean ± SEM was obtained from three independent experiments. n.s., not significant; $*p < 0.05$, $**p < 0.01$, and $***p < 0.001$. (For interpretation of the references to colour in this figure legend, the reader is referred to the Web version of this article.)

ASD-DNs. To confirm this, Ca^{2+} entry into mitochondria was inhibited with RuR, an inhibitor of the mitochondrial calcium uniporter channel complex (mtCU) [25]. In ASD-DNs, RuR inhibited MLT-mediated mitochondrial Ca^{2+} elevation (Figs. S6 and S7). Additionally, RuR blocked the MLT effect on neurite outgrowth of ASD-DNs (Fig. S8). Thus, in ASD-DNs, mitochondrial Ca^{2+} levels were constitutively reduced, which was improved by MTL, leading to acceleration of mitochondrial activation and neurite outgrowth.

3.3. Melatonin was effective in IP3-mediated Ca^{2+} movement from ER to mitochondria in ASD-DNs

ER regulates mitochondrial Ca^{2+} through IP3 receptor (IP3R)-mediated Ca^{2+} movement. The impact of ER on MLT's effects on mitochondrial Ca^{2+} regulation was studied using XestC, an IP3R inhibitor [26]. MLT-induced mitochondrial Ca^{2+} increase in ASD-DNs was inhibited by XestC (Fig. 3A, Fig. S9A). ER Ca^{2+} levels were higher in ASD-DNs than in Ctrl-DNs without treatment but were lowered by MLT, and this effect was blocked by XestC (Fig. 3B, Fig. S9B). This contrasts with mitochondrial Ca^{2+} levels; the consistent decrease in

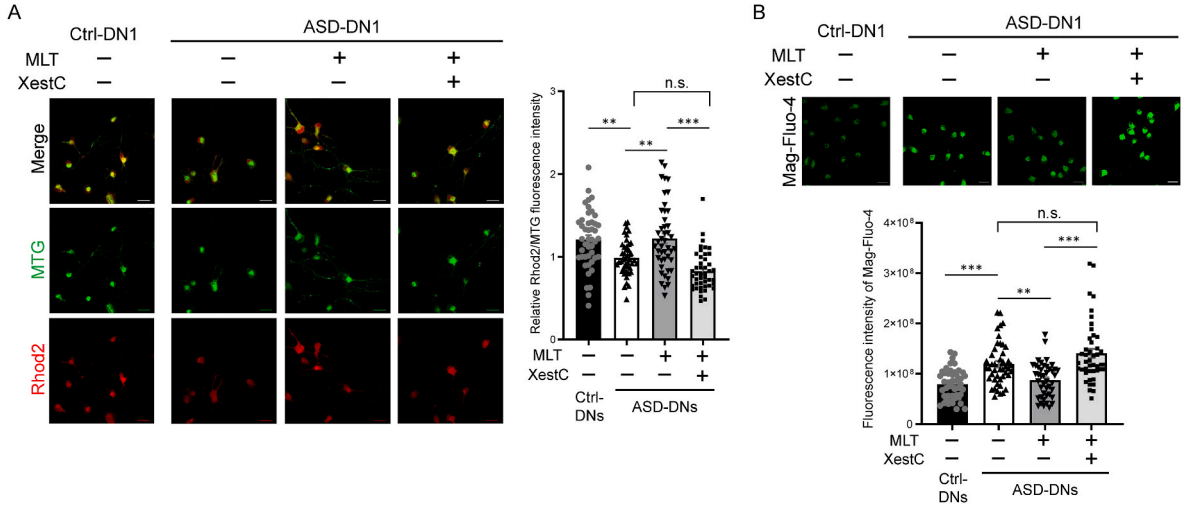

Fig. 3. Inhibition of IP3R suppressed MLT-mediated mitochondrial Ca^{2+} elevation in patient-derived dopaminergic neurons (DNs). SHEDs were differentiated into DNs in the absence or presence of MLT and xestospongin C (XestC), an IP3R inhibitor. (A) DNs stained with MTG and Rhod2 were observed using confocal microscopy. Scale bars = 25 μm. Fluorescence intensity of Rhod2 was divided by that of MTG to measure the Ca^{2+} level per mitochondrion. The mean ± SEM was obtained from three independent experiments. (B) DNs were stained with Mag-Fluo-4 AM and observed using confocal microscopy. Scale bar = 25 μm. Fluorescence intensities of Mag-Fluo-4 AM were measured. The mean ± SEM was obtained from three independent experiments. n.s., not significant; $**p < 0.01$, and $***p < 0.001$.

mitochondrial Ca^{2+} levels in ASD-DNs may relate to a defect in ER-supplied Ca^{2+}, and MLT could improve this by promoting IP3R-mediated Ca^{2+} transfer to mitochondria.

To further investigate, IP3 levels were measured since MT1 and MT2 generate IP3 after activation. IP3 levels were lower in ASD-DNs than in Ctrl-DNs (Fig. 4A). MLT raised IP3 levels in ASD-DNs, which was blocked by LZD (Fig. 4A). MLT-induced reduction of ER Ca^{2+} levels in ASD-DNs was also blocked by LZD (Fig. 4B, Fig. S10). Thus, IP3 was decreased in ASD-DNs, which MLT may target to promote IP3R-mediated Ca^{2+} release from ER to mitochondria (Fig. 4C).

4. Discussion

DNs were differentiated from patient-derived SHEDs with and without MLT to explore MLT's effects on ASD neuropathology. MLT activated MT1 and MT2, which increased IP3-dependent Ca^{2+} movement from ER to mitochondria, improving mitochondrial function and neurite outgrowth in ASD-DNs.

Intracellular Ca^{2+} homeostasis disruption causes neuropsychiatric diseases, including ASD [7], but its molecular mechanisms are unknown. We found that mitochondrial Ca^{2+} levels were lower in ASD-DNs, and Ca^{2+} was accumulated in ER. The ER is essential for Ca^{2+} storage, buffering, and supply [27,28]. IP3R on the ER membrane is a major Ca^{2+} channel [28]. IP3R dysregulation disrupts Ca^{2+} levels in cells, impairing Ca^{2+}-dependent responses. ASD-DNs had lower IP3 levels, which reduced IP3R-mediated Ca^{2+} release from ER, explaining the pathological decrease of mitochondrial Ca^{2+} in ASD-DNs. MLT appeared to improve these deficiencies through MT1 and MT2. GPCRs activate PLCβ, which hydrolyzes phosphatidylinositol 4,5-bisphosphate [29], via Gβγ dimers in a pertussis toxin (PTX)-sensitive $G\alpha_i$-dependent manner [30]. Since both MT1 and MT2 couple with $G\alpha_i$ isoforms [31–34], they might be responsible for IP3 production in ASD-DNs. PLCβ is directly activated by PTX-insensitive $G\alpha_{q/11}$ [30], and MT1 couples with $G\alpha_{q/11}$ isoforms [35], potentially activating IP3 production via this pathway in ASD-DNs. We did not assess Gα isoform selectivity between MT1 and MT2 in ASD-DNs. However, the data suggest that MLT activated MT1 and MT2 to increase PLCβ-dependent IP3 production, compensating for IP3 insufficiency in ASD-DNs.

Impaired IP3-dependent Ca^{2+} movement from ER to mitochondria may cause mitochondrial dysfunction and impede neurite outgrowth in ASD-DNs. Mitochondrial Ca^{2+} is necessary for TCA cycle enzymatic reactions to power electron transport and generate ATP for neurodevelopment [28]. In ASD-DNs, IP3 insufficiency caused reduced mitochondrial Ca^{2+}, MMP, and ATP, suggesting mitochondrial dysfunction. MLT improved mitochondrial function and neurite outgrowth in ASD-DNs, but these effects were reversed by blocking mitochondrial Ca^{2+} entry or MT1/MT2. Thus, developmental defects of ASD-DNs may be linked to IP3-dependent mitochondrial Ca^{2+} homeostasis disruption, which MLT-mediated MT1 and MT2 activation can improve.

Nevertheless, this study has several limitations. It is impossible to generalize the IP3-mediated MLT's effect on DN development to highly heterogeneous ASD population. Further study is required for elucidating the involvement of defects in PLC activation and IP3 metabolic pathways in ASD neuropathology. Additionally, MT1 and MT2 protein expression in ASD-DNs is unknown. The MT1 and MT2 expression ratio may influence therapeutic ligand effects. Third, MLT may regulate cytosolic Ca^{2+} via IP3 production, aiding neurodevelopment in ASD-DNs. Fourth, MLT levels and distribution in ASD brains have not been fully explored. These studies are essential to understand MLT's clinical role in neurodevelopment.

In conclusion, MLT supplementation improves ASD-DN development by regulating IP3-mediated mitochondrial Ca^{2+} homeostasis via MT1 and MT2 activation. MLT is released in sync with the circadian rhythm *in vivo*. Thus, MLT treatment of ASD-DNs *in vitro* may replicate the nocturnal environment with high MLT levels in the brain. In contrast, cell culture without MLT may mimic nocturnal conditions, where MLT is lacking in the brain due to sleep deprivation or circadian rhythm disruption as observed in ASD. The current data potentially contribute to an extended understanding of MLT on a molecular level, and to translational research for children with ASD suffering from sleep deprivation.

Author contributions

Conceptualization, K.M. and T.K.; methodology, S.D., H.K., and H.S.; validation, T.K., L.W., J.K., Y.H., X.S., and Y.I.; analysis, S.D. and T.K.; writing—original draft preparation, S.D., T.K., and K.M.; writing—review and editing, H.K., Y.S., and K.M.; supervision, T.A.K., Y.S., and S. O.; project administration, S.F. and K.M.; funding acquisition, T.K., Y.H., and K.M. All authors have read and agreed to the published version of

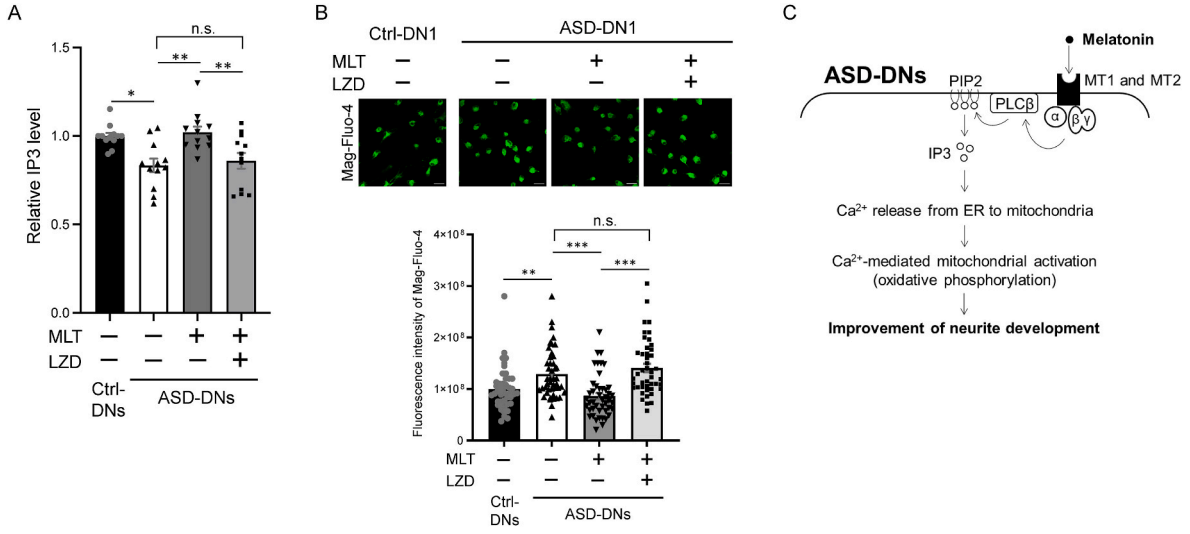

Fig. 4. MLT is involved in Ca^{2+} release from ER to mitochondria via IP3 production in patient-derived dopaminergic neurons (DNs). SHEDs were differentiated into DNs in the absence or presence of MLT and LZD. (A) IP3 levels in DNs were measured. The mean ± SEM was obtained from three independent experiments. (B) DNs were stained with Mag-Fluo-4 AM and observed using confocal microscopy. Scale bar = 25 μm. Fluorescence intensities of Mag-Fluo-4 AM were measured. The mean ± SEM was obtained from three independent experiments. n.s., not significant; $*p < 0.05$, $**p < 0.01$, and $***p < 0.001$. (C) Schematic of the tentative pathway of MLT effects on neurite development in ASD-DNs.

the manuscript.

Funding

This work was supported by the Japan Society for the Promotion of Science [KAKENHI; grant numbers JP20K18785, JP21K17163, JP23K09439 and JP23K09417], and the Japan Science and Technology Agency SPRING [grant number JPMJSP2136].

Data availability statement

Data supporting the findings of this study are available in the article and its supplementary materials.

Declaration of competing interest

The authors declare that they have no known competing financial interests or personal relationships that could have appeared to influence the work reported in this paper.

Acknowledgments

We thank the members of the Department of Pediatric Dentistry and Special Needs Dentistry at Kyushu University Hospital for their valuable suggestions, technical support, and materials. We appreciate the technical assistance provided by the Research Support Center at the Research Center for Human Disease Modeling, Kyushu University Graduate School of Medical Sciences. This work was supported by JST SPRING.

Appendix A. Supplementary data

Supplementary data to this article can be found online at https://doi.org/10.1016/j.bbrc.2023.09.050.

References

[1] C. Lord, T.S. Brugha, T. Charman, J. Cusack, G. Dumas, T. Frazier, E.J.H. Jones, R. M. Jones, A. Pickles, M.W. State, J.L. Taylor, J. Veenstra-VanderWeele, Autism spectrum disorder, Nat. Rev. Dis. Prim. 6 (2020) 5.
[2] Y. Sztainberg, H.Y. Zoghbi, Lessons learned from studying syndromic autism spectrum disorders, Nat. Neurosci. 19 (2016) 1408–1417.
[3] P. Chaste, M. Leboyer, Autism risk factors: genes, environment, and gene-environment interactions, Dialogues Clin. Neurosci. 14 (2012) 281–292.
[4] F. Hollis, A.K. Kanellopoulos, C. Bagni, Mitochondrial dysfunction in autism spectrum disorder: clinical features and perspectives, Curr. Opin. Neurobiol. 45 (2017) 178–187.
[5] M. Nguyen, A. Roth, E.J. Kyzar, M.K. Poudel, K. Wong, A.M. Stewart, A.V. Kalueff, Decoding the contribution of dopaminergic genes and pathways to autism spectrum disorder (ASD), Neurochem. Int. 66 (2014) 15–26.
[6] D. Pavăl, I.V. Micluția, The dopamine hypothesis of autism spectrum disorder revisited: current status and future prospects, Dev. Neurosci. 43 (2021) 73–83.
[7] R.L. Nguyen, Y.V. Medvedeva, T.E. Ayyagari, G. Schmunk, J.J. Gargus, Intracellular calcium dysregulation in autism spectrum disorder: an analysis of converging organelle signaling pathways, Biochim. Biophys. Acta Mol. Cell Res. 1865 (2018) 1718–1732.
[8] H.T.N. Nguyen, H. Kato, K. Masuda, H. Yamaza, Y. Hirofuji, H. Sato, T.T.M. Pham, F. Takayama, Y. Sakai, S. Ohga, T. Taguchi, K. Nonaka, Impaired neurite development associated with mitochondrial dysfunction in dopaminergic neurons differentiated from exfoliated deciduous tooth-derived pulp stem cells of children with autism spectrum disorder, Biochem. Biophys. Rep. 16 (2018) 24–31.
[9] Z.Y. Wu, S.D. Huang, J.J. Zou, Q.X. Wang, M. Naveed, H.N. Bao, W. Wang, K. Fukunaga, F. Han, Autism spectrum disorder (ASD): disturbance of the melatonin system and its implications, Biomed. Pharmacother. 130 (2020), 110496.
[10] G. Missig, C.J. McDougle, W.A. Carlezon Jr., Sleep as a translationally-relevant endpoint in studies of autism spectrum disorder (ASD), Neuropsychopharmacology 45 (2020) 90–103.
[11] R.J. Reiter, D.X. Tan, S.J. Kim, M.H. Cruz, Delivery of pineal melatonin to the brain and SCN: role of canaliculi, cerebrospinal fluid, tanycytes and Virchow-Robin perivascular spaces, Brain Struct. Funct. 219 (2014) 1873–1887.
[12] N.S. Foulkes, J. Borjigin, S.H. Snyder, P. Sassone-Corsi, Rhythmic transcription: the molecular basis of circadian melatonin synthesis, Trends Neurosci. 20 (1997) 487–492.
[13] J. Liu, S.J. Clough, A.J. Hutchinson, E.B. Adamah-Biassi, M. Popovska-Gorevski, M. L. Dubocovich, MT1 and MT2 melatonin receptors: a therapeutic perspective, Annu. Rev. Pharmacol. Toxicol. 56 (2016) 361–383.
[14] B. Rzepka-Migut, J. Paprocka, Efficacy and safety of melatonin treatment in children with autism spectrum disorder and attention-deficit/hyperactivity disorder-a review of the literature, Brain Sci. 10 (2020) 219.
[15] S.B. Ahmad, A. Ali, M. Bilal, S.M. Rashid, A.B. Wani, R.R. Bhat, M.U. Rehman, Melatonin and health: insights of melatonin action, biological functions, and associated disorders, Cell. Mol. Neurobiol. (2023) 1–22.
[16] C. Ekmekcioglu, Melatonin receptors in humans: biological role and clinical relevance, Biomed. Pharmacother. 60 (2006) 97–108.
[17] G.T. Huang, S. Gronthos, S. Shi, Mesenchymal stem cells derived from dental tissues vs. those from other sources: their biology and role in regenerative medicine, J. Dent. Res. 88 (2009) 792–806.
[18] M. Miura, S. Gronthos, M. Zhao, B. Lu, L.W. Fisher, P.G. Robey, S. Shi, SHED: stem cells from human exfoliated deciduous teeth, Proc. Natl. Acad. Sci. U.S.A. 100 (2003) 5807–5812.
[19] H. Fujii, K. Matsubara, K. Sakai, M. Ito, K. Ohno, M. Ueda, A. Yamamoto, Dopaminergic differentiation of stem cells from human deciduous teeth and their therapeutic benefits for Parkinsonian rats, Brain Res. 1613 (2015) 59–72.
[20] D. Majumdar, M. Kanafi, R. Bhonde, P. Gupta, I. Datta, Differential neuronal plasticity of dental pulp stem cells from exfoliated deciduous and permanent teeth towards dopaminergic neurons, J. Cell. Physiol. 231 (2016) 2048–2063.
[21] E. Arenas, M. Denham, J.C. Villaescusa, How to make a midbrain dopaminergic neuron, Development 142 (2015) 1918–1936.
[22] K. Masuda, X. Han, H. Kato, H. Sato, Y. Zhang, X. Sun, Y. Hirofuji, H. Yamaza, A. Yamada, S. Fukumoto, Dental pulp-derived mesenchymal stem cells for modeling genetic disorders, Int. J. Mol. Sci. 22 (2021) 2269.
[23] X. Sun, S. Dong, H. Kato, J. Kong, Y. Ito, Y. Hirofuji, H. Sato, T.A. Kato, Y. Sakai, S. Ohga, S. Fukumoto, K. Masuda, Mitochondrial calcium-triggered oxidative stress and developmental defects in dopaminergic neurons differentiated from deciduous teeth-derived dental pulp stem cells with MFF insufficiency, Antioxidants 11 (2022) 1361.
[24] M.L. Dubocovich, Luzindole (N-0774): a novel melatonin receptor antagonist, J. Pharmacol. Exp. Therapeut. 246 (1988) 902–910.
[25] K. Márta, P. Hasan, M. Rodríguez-Prados, M. Paillard, G. Hajnóczky, Pharmacological inhibition of the mitochondrial Ca(2+) uniporter: relevance for pathophysiology and human therapy, J. Mol. Cell. Cardiol. 151 (2021) 135–144.
[26] J. Gafni, J.A. Munsch, T.H. Lam, M.C. Catlin, L.G. Costa, T.F. Molinski, I.N. Pessah, Xestospongins: potent membrane permeable blockers of the inositol 1,4,5-trisphosphate receptor, Neuron 19 (1997) 723–733.
[27] R. Rizzuto, M. Brini, M. Murgia, T. Pozzan, Microdomains with high Ca2+ close to IP3-sensitive channels that are sensed by neighboring mitochondria, Science 262 (1993) 744–747.
[28] A. Rossi, P. Pizzo, R. Filadi, Calcium, mitochondria and cell metabolism: a functional triangle in bioenergetics, Biochim. Biophys. Acta Mol. Cell Res. 1866 (2019) 1068–1078.
[29] D.C. New, S.T. Tsim, Y.H. Wong, G protein-linked effector and second messenger systems involved in melatonin signal transduction, Neurosignals 12 (2003) 59–70.
[30] M.J. Rebecchi, S.N. Pentyala, Structure, function, and control of phosphoinositide-specific phospholipase C, Physiol. Rev. 80 (2000) 1291–1335.
[31] F. Roka, L. Brydon, M. Waldhoer, A.D. Strosberg, M. Freissmuth, R. Jockers, C. Nanoff, Tight association of the human Mel(1a)-melatonin receptor and G(i): precoupling and constitutive activity, Mol. Pharmacol. 56 (1999) 1014–1024.
[32] R.S. MacKenzie, M.A. Melan, D.K. Passey, P.A. Witt-Enderby, Dual coupling of MT (1) and MT(2) melatonin receptors to cyclic AMP and phosphoinositide signal transduction cascades and their regulation following melatonin exposure, Biochem. Pharmacol. 63 (2002) 587–595.
[33] S.M. Reppert, D.R. Weaver, T. Ebisawa, Cloning and characterization of a mammalian melatonin receptor that mediates reproductive and circadian responses, Neuron 13 (1994) 1177–1185.
[34] S.M. Reppert, C. Godson, C.D. Mahle, D.R. Weaver, S.A. Slaugenhaupt, J.F. Gusella, Molecular characterization of a second melatonin receptor expressed in human retina and brain: the Mel1b melatonin receptor, Proc. Natl. Acad. Sci. U.S.A. 92 (1995) 8734–8738.
[35] L. Brydon, F. Roka, L. Petit, P. de Coppet, M. Tissot, P. Barrett, P.J. Morgan, C. Nanoff, A.D. Strosberg, R. Jockers, Dual signaling of human Mel1a melatonin receptors via G(i2), G(i3), and G(q/11) proteins, Mol. Endocrinol. 13 (1999) 2025–2038.

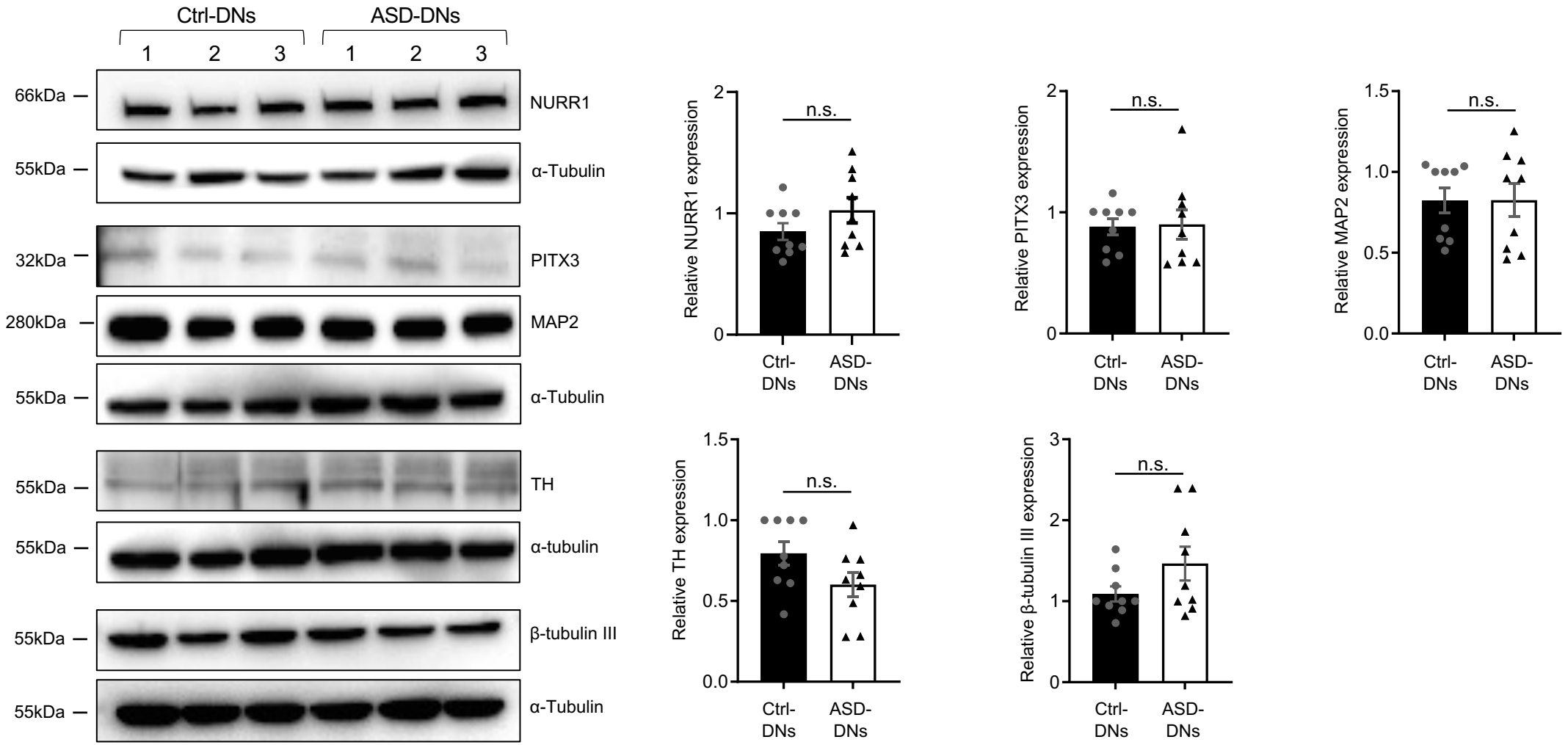

Supplementary Figure S1

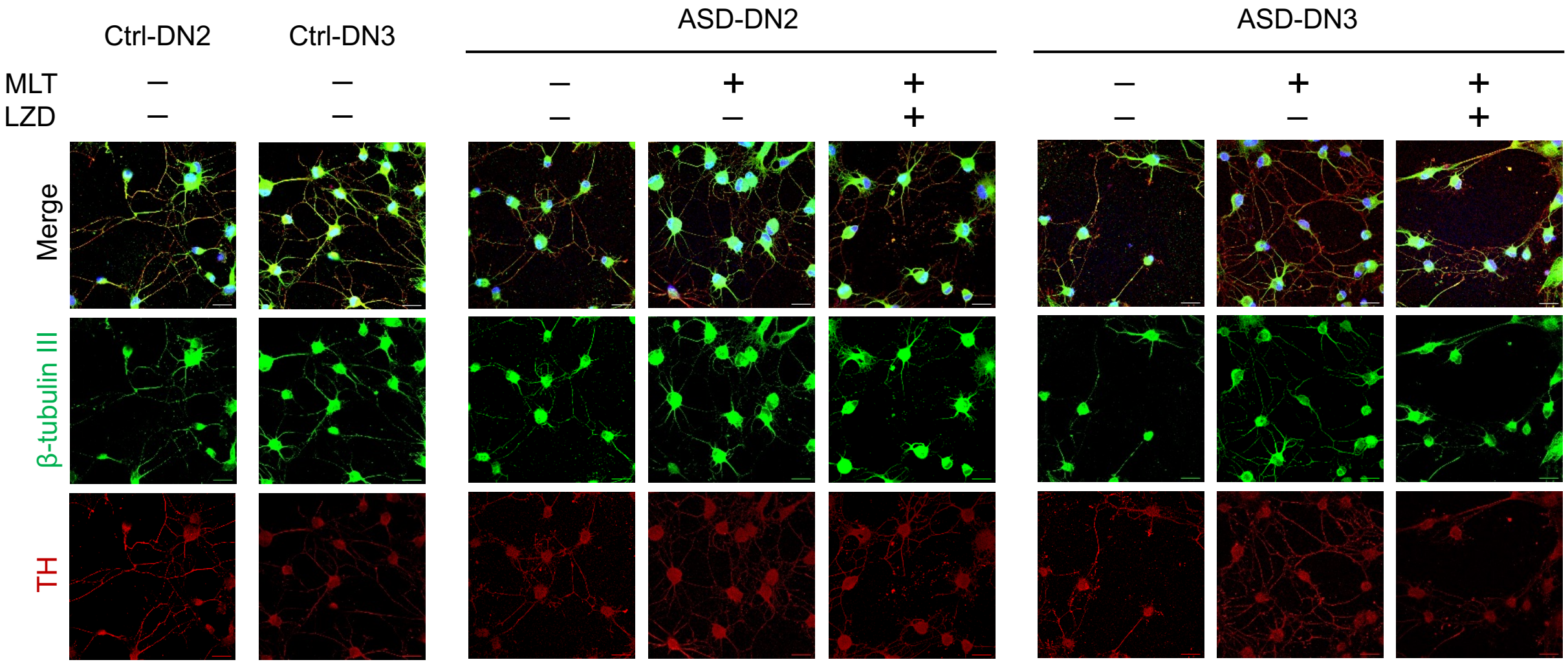

Supplementary Figure S2

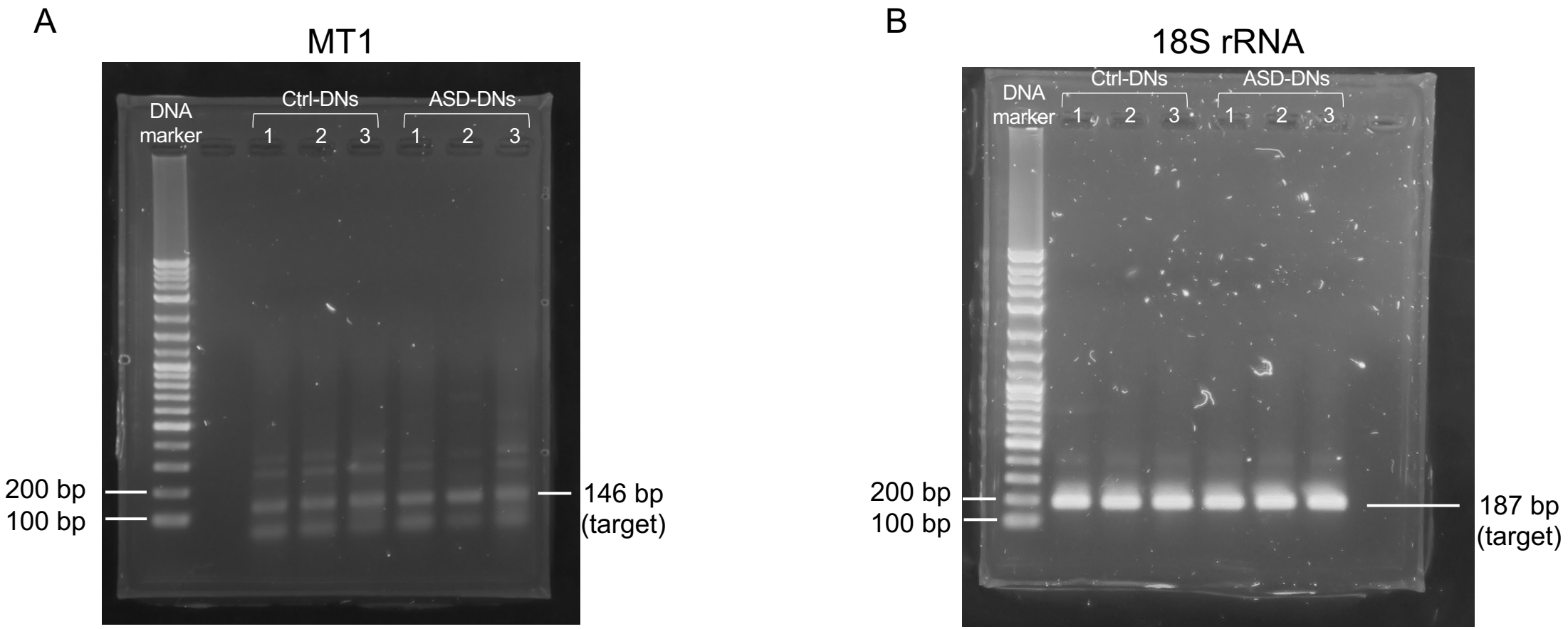

Supplementary Figure S3

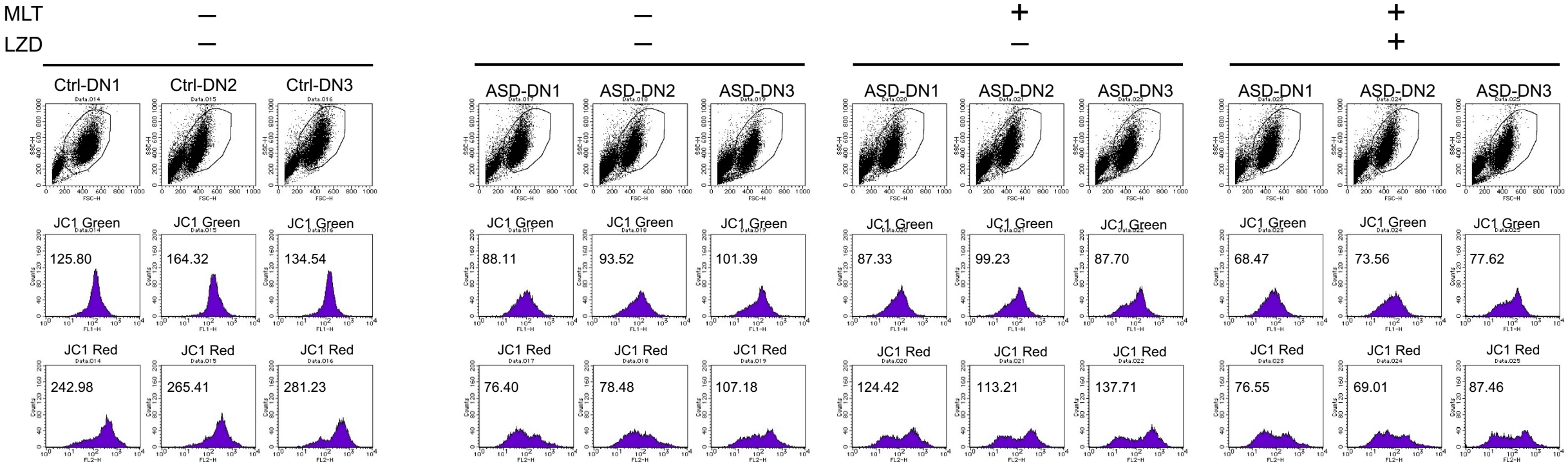

Supplementary Figure S4

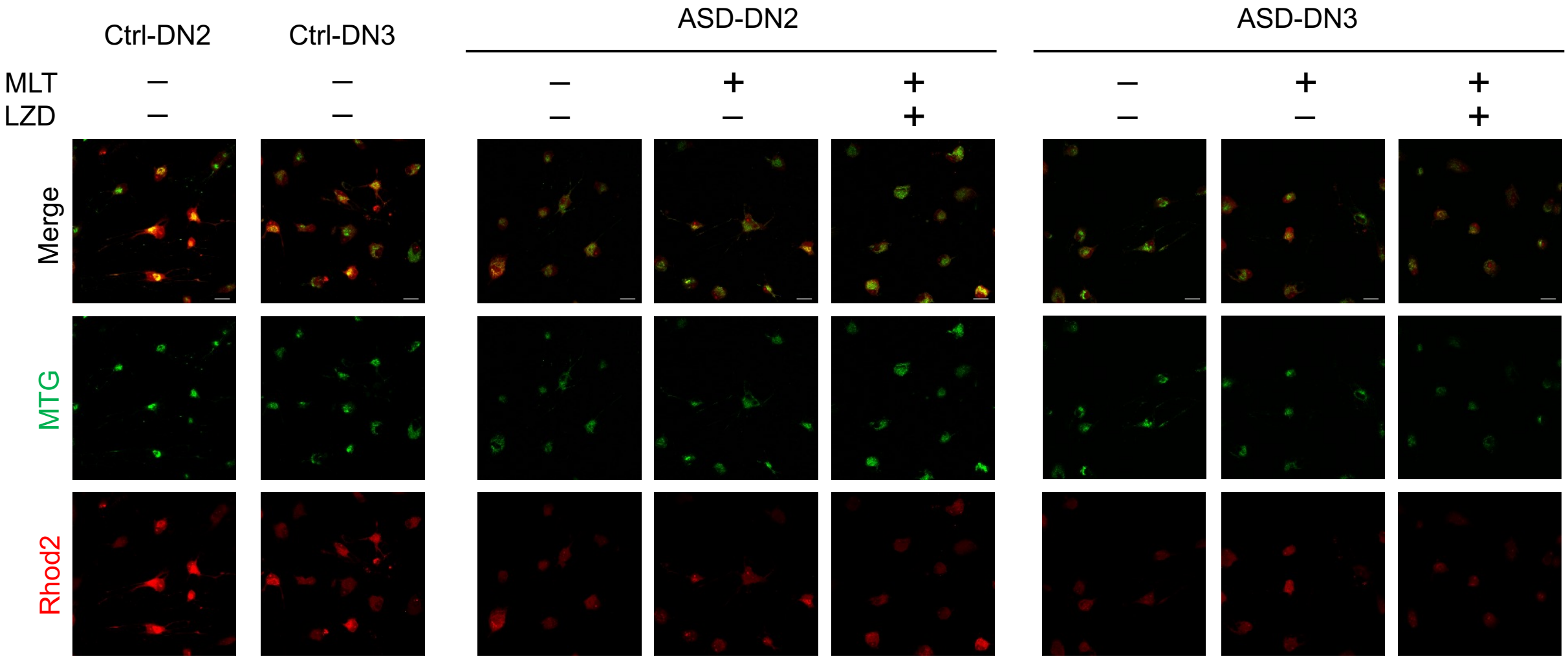

Supplementary Figure S5

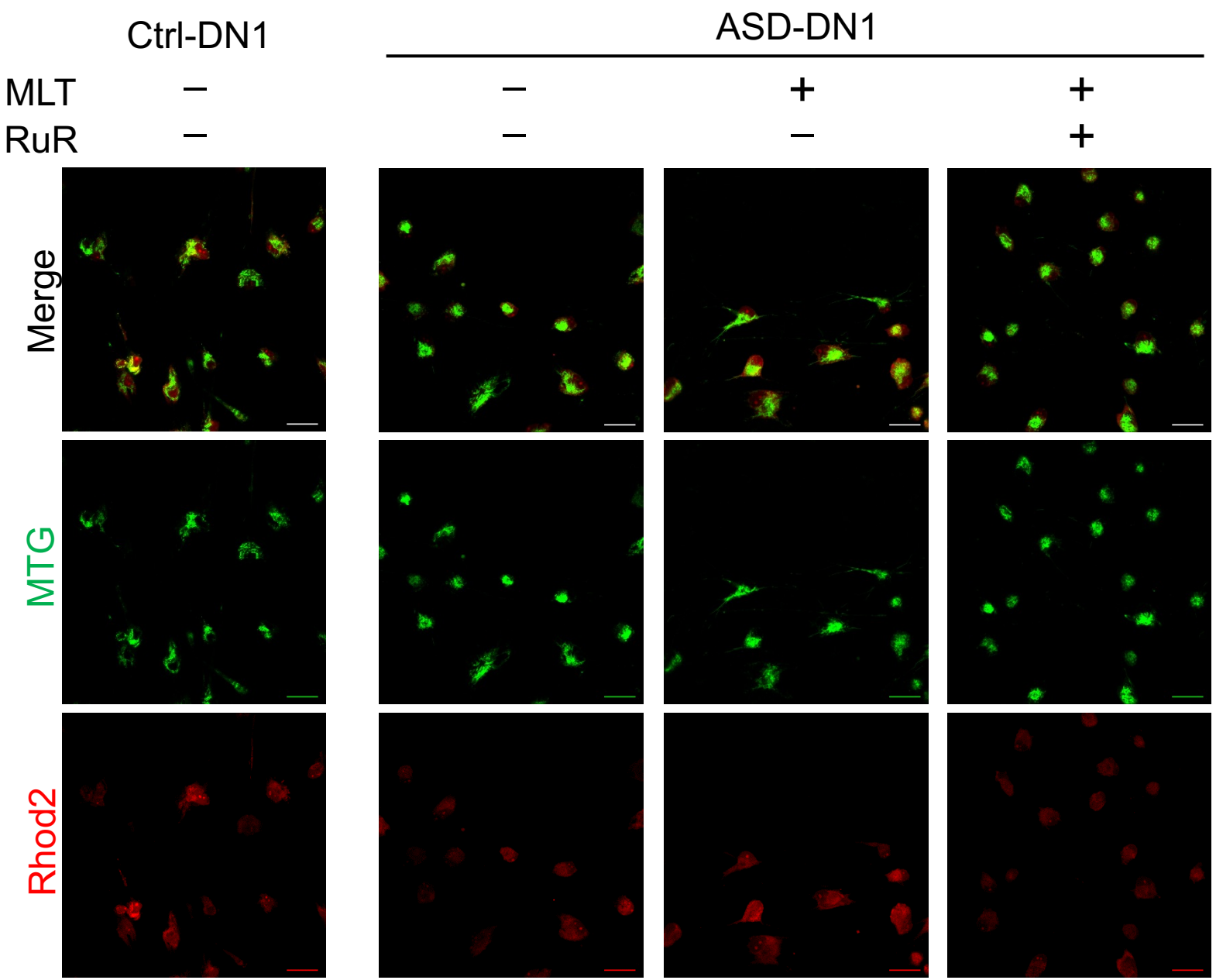

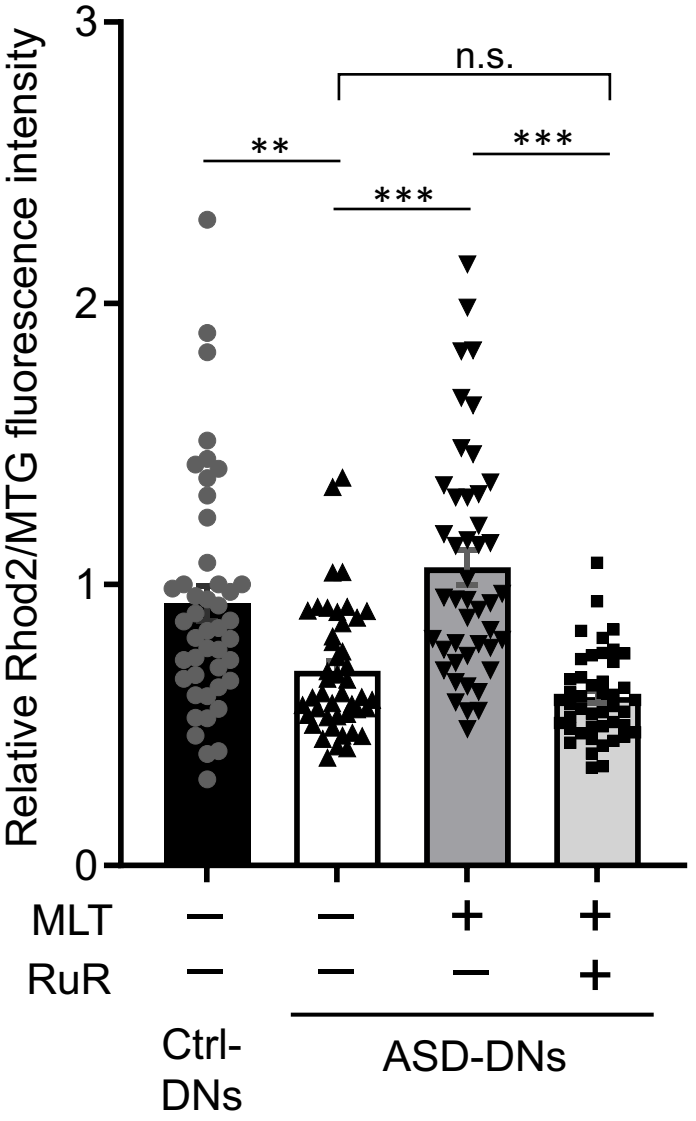

Supplementary Figure S6

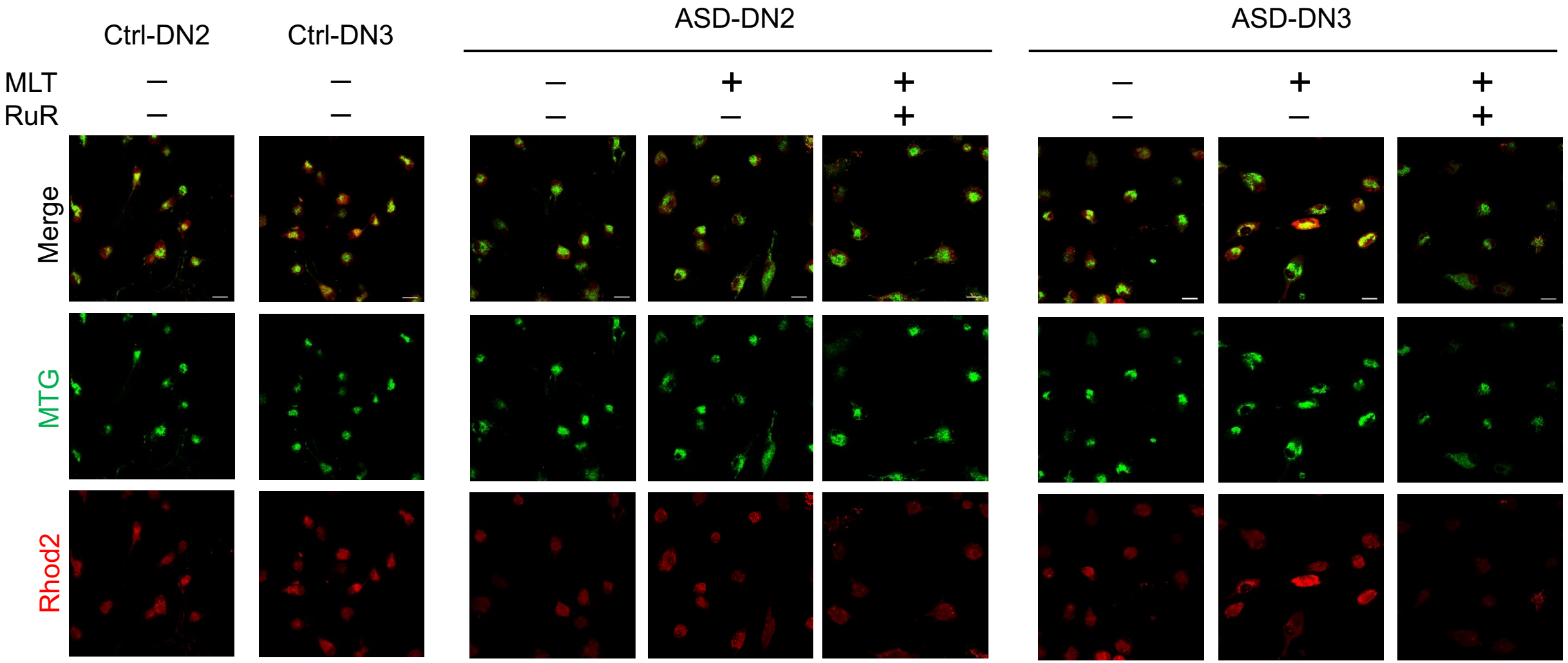

Supplementary Figure S7

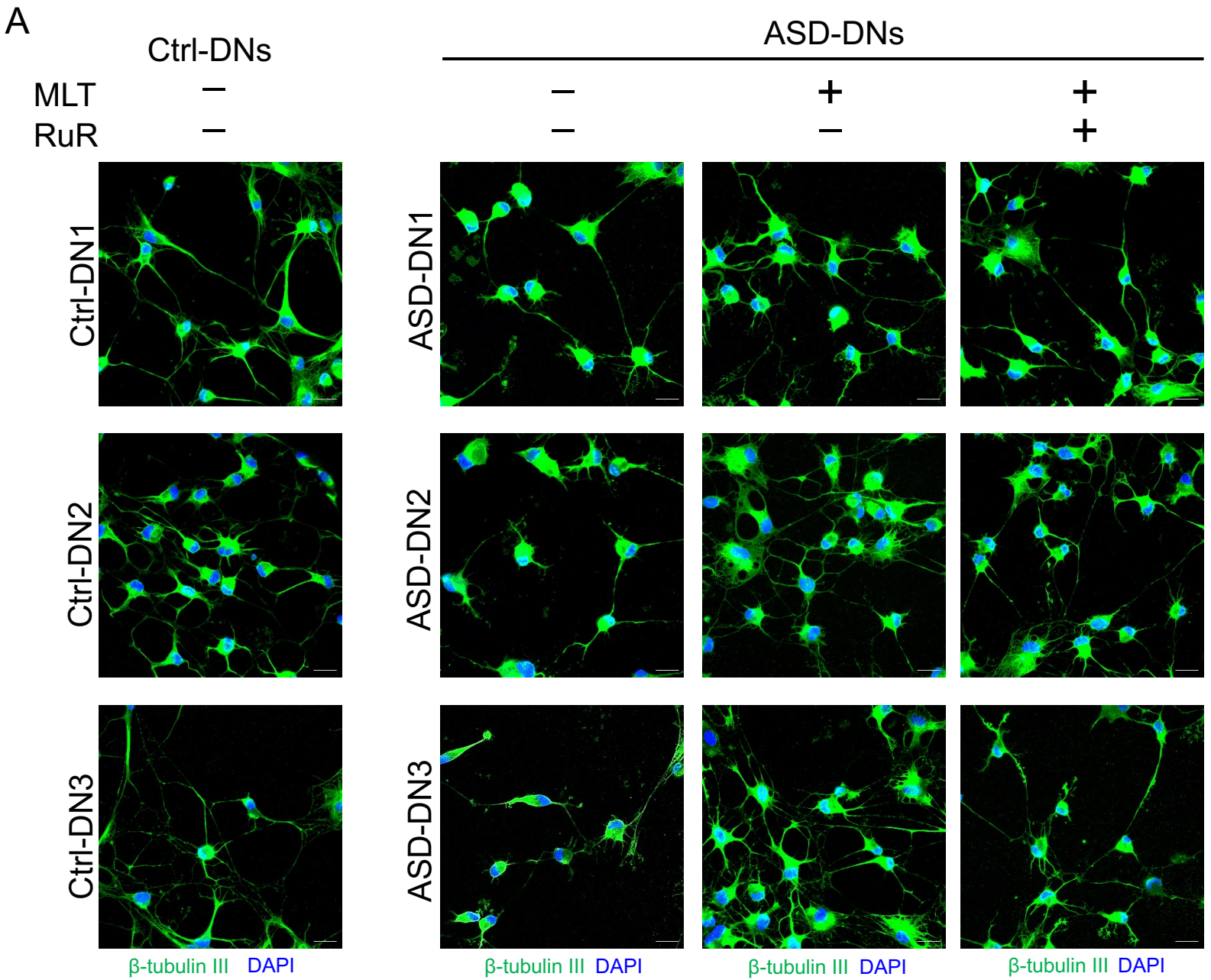

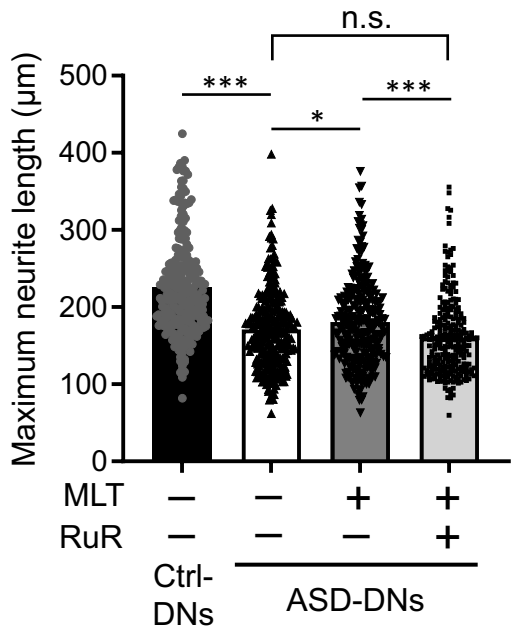

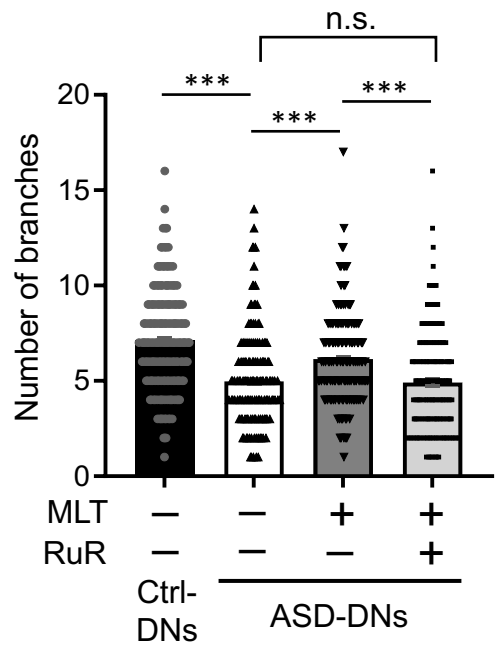

Supplementary Figure S8

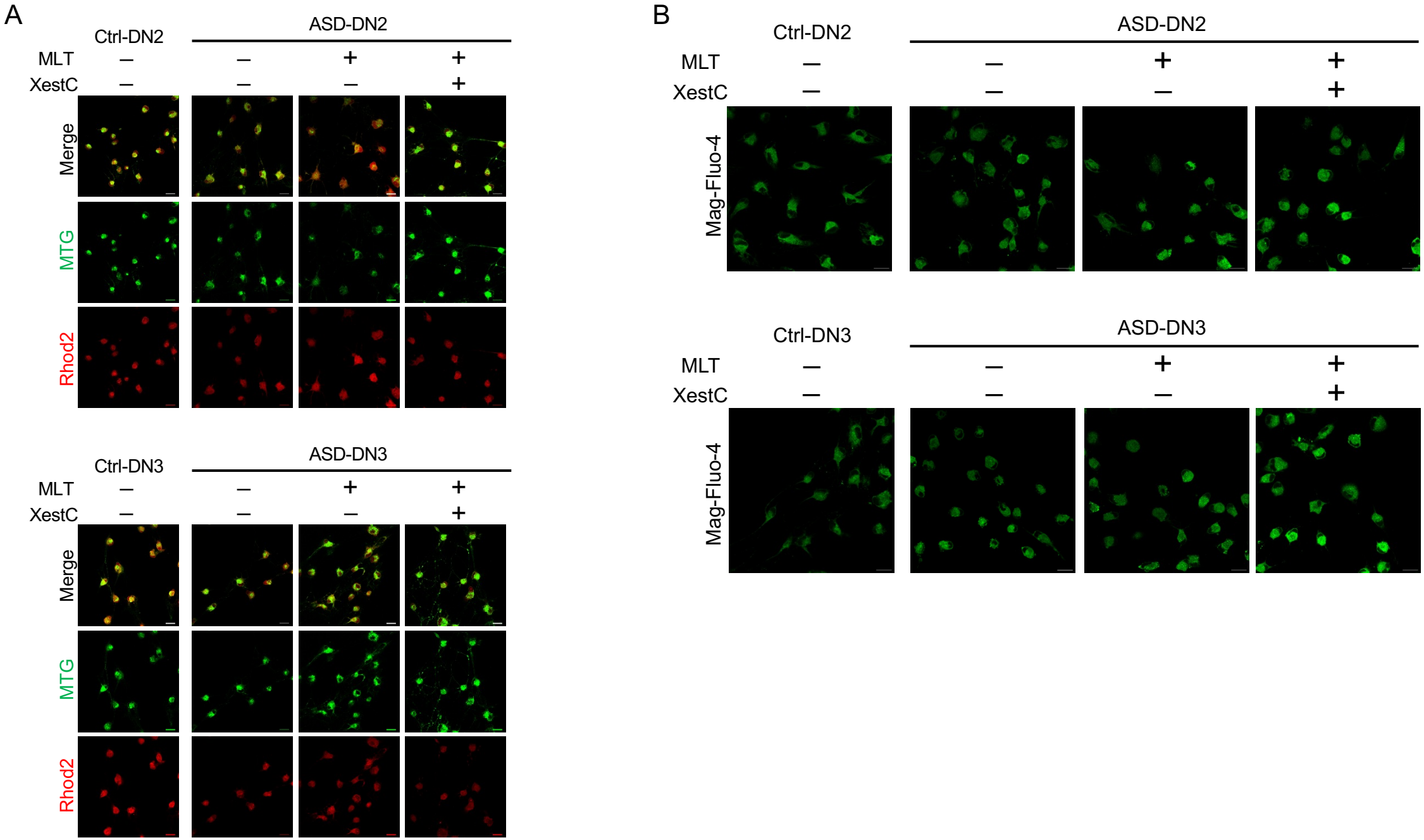

Supplementary Figure S9

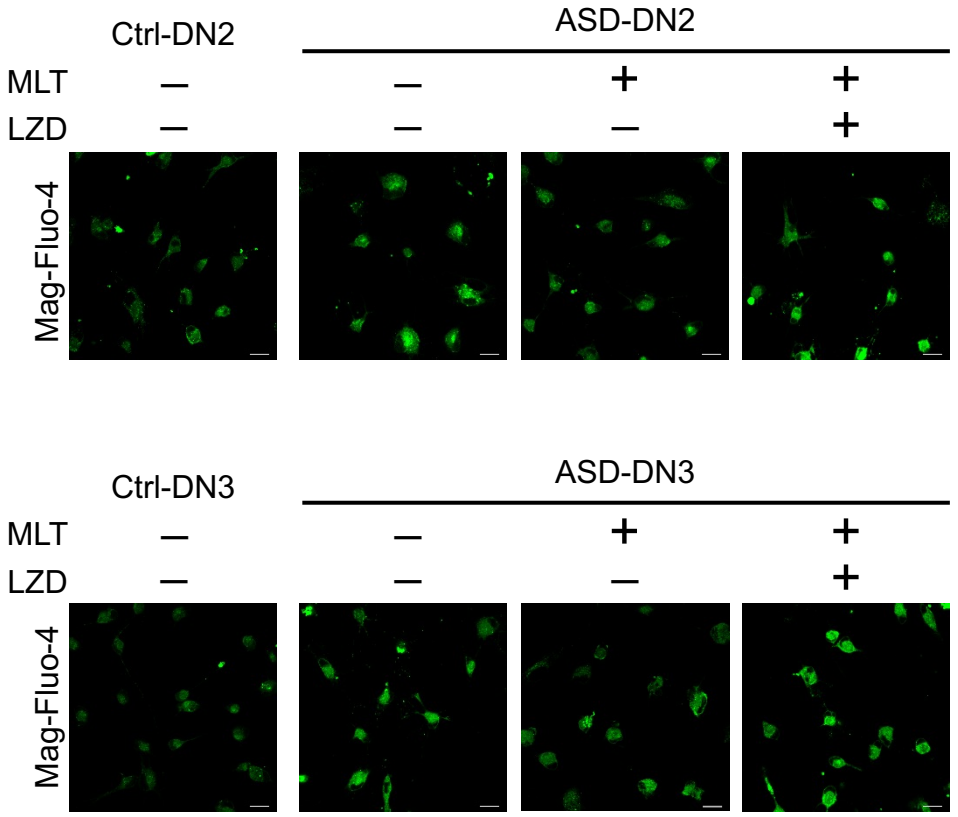

Supplementary Figure S10